



ELSEVIER

Available online at [www.sciencedirect.com](http://www.sciencedirect.com)

Journal of Magnetism and Magnetic Materials 320 (2008) 1631–1638

[www.elsevier.com/locate/jmmm](http://www.elsevier.com/locate/jmmm)

# Structural and magnetic features of heterogeneously nucleated Fe-oxide nanoparticles

K. Simeonidis<sup>a</sup>, S. Mourdikoudis<sup>a</sup>, I. Tsiaoussis<sup>a</sup>, M. Angelakeris<sup>a</sup>,  
C. Dendrinou-Samara<sup>b</sup>, O. Kalogirou<sup>a,\*</sup>

<sup>a</sup>Department of Physics, Aristotle University of Thessaloniki, Thessaloniki 54124, Greece

<sup>b</sup>Department of Chemistry, Aristotle University of Thessaloniki, Thessaloniki 54124, Greece

Received 6 December 2007; received in revised form 10 January 2008

Available online 24 January 2008

## Abstract

Iron oxide nanoparticles of diameter 14 nm were synthesized by applying Pt seed-assisted heterogeneous thermal decomposition of  $\text{Fe}(\text{CO})_5$  in a two-stage procedure. The intense heating treatment resulted in a remarkable mean volume increment compared to previous studies. This method is able to control the nanoparticle mean diameter, keeping the demand for thermal energy at low levels. High-resolution electron microscopy images and the corresponding electron diffraction patterns revealed the appearance of a  $\text{FePt}_3$  core in each nanoparticle, surrounded by highly crystallized inverse spinel  $\text{Fe}_3\text{O}_4$  formed after atmospheric oxidation, as shown by a combination of X-ray diffraction and chemical analysis. Magnetic measurements indicated that the presence of Pt-rich core does not cause any visible modification to the values of saturation magnetization and anisotropy constant of nanoparticles, compared to homogeneously nucleated iron oxide particles of the same size.

© 2008 Elsevier B.V. All rights reserved.

PACS: 75.50.Tt; 61.46.Df; 75.75.+a; 75.50.Bb

Keywords: Iron oxide; Nanoparticle; Heterogeneous nucleation; Core-shell; FePt

## 1. Introduction

Controllable synthesis and assembly of magnetic nanoparticles has recently received special attention. Their novel or enhanced physical properties, compared to the bulk state, arise mainly due to finite size and surface effects, which dominate the magnetic behavior of individual nanoparticles. In particular, iron oxide nanoparticles, usually maghemite and magnetite, have gained much interest because of their applicability in biomedical fields such as magnetic resonance imaging (MRI), magnetic fluid hyperthermia, targeted drug delivery, magnetic cell separation and magnetorelaxometry [1–5]. Moreover, they can be used as basic components in technological applications like magnetic recording and permanent magnets [6,7]. In order to override the difficulties following miniaturization in the

first case or improve energy product in the second, binary nanocomposite systems are a promising approach [8,9].

Despite significant progress in the development of synthetic routes, further research is needed to optimize or revise the preparation methods and characterization techniques of the nanoparticles. Among the bottom-up methods, thermal decomposition of metal precursors in an organic solvent is used by many scientists who work on nanoparticle systems [10]. The relative technical simplicity, low cost and efficient control of the size, shape, monodispersity and desired crystalline structure of the synthesized nanoparticles are the major advantages of the aforementioned method.

Uniform iron oxide particles are usually prepared via homogeneous nucleation reactions. The decomposition or reduction of iron precursors in the presence of surfactants often yields nanoparticles with narrow size distribution and good crystallinity. In order to achieve high monodispersity, separation of the nucleation stage and the growth of the

\*Corresponding author. Tel.: +30 2310 998148; fax: +30 2310 998003.

E-mail address: [orestis.kalogirou@physics.auth.gr](mailto:orestis.kalogirou@physics.auth.gr) (O. Kalogirou).

nuclei is an essential condition. However, the use of high surfactant concentration favors the formation of intermediate complexes between metal ions and surfactant molecules, which increases the nucleation temperature [11]. A better control of the average size of metal particles can be obtained by seeding the reactive medium with other element particles acting like catalytic centers for the building of iron nanocrystals. The reduction of total surface energy results in lesser thermal energy requirements for iron nucleation compared to the homogeneous mechanism. Furthermore, much lower surfactant concentration is needed and therefore, the temperature at which decomposition of precursor initiates, decreases dramatically. Thus, during a heterogeneous pathway, nucleation and growth procedures are completely separated, while it is possible to work at somewhat lower temperatures [12].

In this work we describe the preparation of 14 nm sized iron oxide nanoparticles obtained by heterogeneous nucleation synthesis. Platinum seeds are used as the nucleating agent. Structural and magnetic characterization revealed a two-phase arrangement (core-shell) of the nanoparticles under study, with interesting technological features if properly tailored.

## 2. Experimental

Iron oxide nanoparticles were synthesized by a variation of the heterogeneous nucleation method of Farrell et al. [13]. The reaction conditions were optimized to produce larger nanoparticles. Thus, longer heating times were used. The procedure followed in our case consists of two stages: growth of iron on platinum seeds and size increment by adding excess of iron precursor.

For the preparation of 14 nm sized iron oxide nanoparticles, platinum nuclei were initially formed after reduction of 0.01 mmol Pt(acac)<sub>2</sub> (Aldrich, 99.99%) by 0.58 mmol 1,2-hexadecanediol (Aldrich, 90%) in the presence of 1 mmol oleic acid (Aldrich, 90%) and 1 mmol oleylamine (Fluka, >70%) into 15 ml dioctyl ether (Fluka, >97%) solution under an Ar atmosphere. Then the mixture was heated at a 6 °C min<sup>-1</sup> rate to 100 °C and 1.5 mmol Fe(CO)<sub>5</sub> (Aldrich, 99.999%) was added. The yellow solution was further heated at the same rate until reflux at 290 °C where it remained for 10 min before cooling. During this process, the color of the solution gradually became black at about 180 °C, indicating the formation of iron nanoparticles.

The solution was diluted by 15 ml dioctyl ether and 9 mmol Fe(CO)<sub>5</sub> were added at 100 °C during reheating. The mixture was heated to reflux point observed at 285 °C and kept at this temperature for 20 min. After cooling to room temperature, ethanol was added to yield a black precipitate, which was then separated by centrifugation. The final product of this process was diluted in *n*-hexane with additional surfactant quantities and kept under a dry air environment.

Maintaining the temperature at the reflux point for a short period of time, in both stages, leads to a remarkable growth of the diameter over the reported 7 nm [13]. However, the formation of large nanoparticles by the method described resulted in a negligible variation of the diameter standard deviation.

The structural properties of iron oxide nanoparticles were analyzed by powder X-ray diffraction (XRD) with a Philips PW 1820 diffractometer under CuK $\alpha$  radiation (1.5406 Å). Information concerning the size distribution and the arrangement of nanoparticles was obtained by high-resolution transmission electron microscopy (HRTEM). The specimens for HRTEM analysis were prepared by room temperature deposition of *n*-hexane dispersions of nanoparticles on carbon-coated copper grids. HRTEM images were acquired using a JEOL 2011 at an accelerating voltage of 200 kV. Additional structural analysis was carried out from the corresponding selected area electron diffraction (SAED) patterns. The existence of surfactant coating on the magnetic nanoparticle surface was investigated using a Fourier transform infrared (FT-IR) spectrometer (Perkin-Elmer FT-IR 1650). Transmission IR spectra with baseline corrections were taken for the analysis. Nanoparticle powder was dried and pelletized with KBr powder for the FT-IR study. Quantitative determination of the surfactant percentage and any phase transformations during heating were studied by thermogravimetric analysis (TGA) in a SETARAM SetSys-1200 instrument from room temperature to 1000 °C at a heating rate of 10 °C min<sup>-1</sup> under a nitrogen atmosphere.

Magnetic hysteresis loops were carried out in the temperature range of 5–300 K using a MPMS-5 Quantum Design SQUID magnetometer. The zero-field cooled (ZFC) curve was obtained by cooling the system in zero magnetic field to 5 K and then applying a constant field of 100 Oe while increasing the temperature to 300 K. For the field-cooled (FC) curve the sample was cooled under the same magnetic field and magnetization was measured in the direction of increasing temperature. Magnetization values were normalized to iron oxide content determined by a chemical analysis method [14].

## 3. Results and discussion

### 3.1. XRD analysis

The XRD pattern of the obtained nanoparticles at the first and second stage, given in Fig. 1, reveals the existence of a spinel-structured iron oxide. This indicates complete oxidation of iron after exposing nanoparticles to atmosphere, though the exact product of this process is very difficult to be identified due to the similar crystal structures of Fe<sub>3</sub>O<sub>4</sub> and  $\gamma$ -Fe<sub>2</sub>O<sub>3</sub>. The absence of platinum or iron-platinum alloy peaks is attributed to the low molar ratio of platinum precursor in the reaction (Fe:Pt  $\approx$  1000:1). The weak diffraction signal of coated Pt alloy has been observed even in FePt/Fe<sub>3</sub>O<sub>4</sub> core-shell nanoparticles,

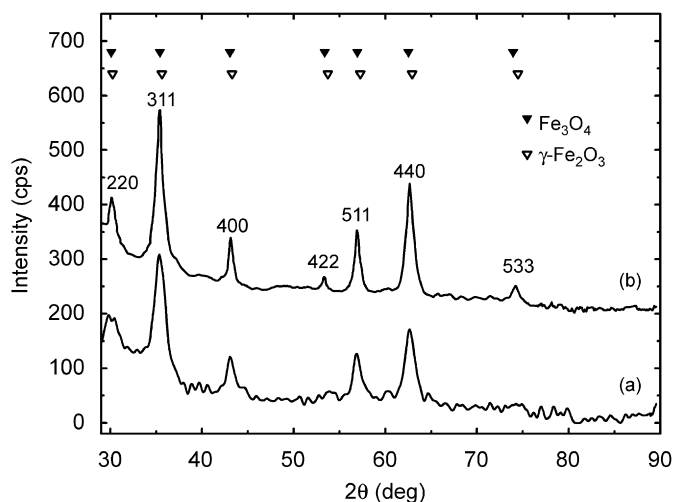


Fig. 1. X-ray powder diffraction patterns of heterogeneously nucleated iron oxide nanoparticles after first stage (a) and second stage (b) of growth. Symbols represent magnetite (▼) and maghemite (▽) peaks.

although the platinum percentage is many times higher than in our case [15]. Applying Scherrer's formula for the (3 1 1) iron oxide peak, the size of nanocrystals before and after the addition of  $\text{Fe}(\text{CO})_5$  excess was calculated as  $8.4 \pm 1.1$  and  $12.9 \pm 1.5$  nm, respectively.

### 3.2. HRTEM

Low-magnification HRTEM images of the sample (Figs. 2(a) and (b)) are consistent with the XRD analysis results concerning nanoparticle size. In the case of nanoparticles formed during the first stage (Fig. 2(b)), the average size was 9.1 nm with an 11% standard deviation, while after the further-growth process (Fig. 2(a)) it was 13.6 nm with a 17% deviation. The iron oxide nanocrystal size exported by Scherrer's formula appears slightly different from the value obtained by TEM analysis due to the existence of a Pt core, as explained below.

In a typical region of the final product, two types of nanoparticles are observed: large 14 nm nanoparticles consisting of a dark core of about 3 nm diameter surrounded by a light-colored thick shell and smaller 8 nm single-phase nanoparticles. This type of core-shell nanoparticles is the result of heterogeneous growth of iron on platinum seeds. Platinum participates in the reduction of surface energy for iron nucleation initiation but is not recovered at the end of the reaction. The core appears darker due to the higher electron density of Pt and it is not necessarily centered. The same situation is described for Au/ $\text{Fe}_3\text{O}_4$  "dumbbell-like" nanoparticles [16] and derives from induced charge compensation during Fe growth in a non-polar solvent like dioctyl ether. The core reaches 8 nm in certain individual nanoparticles, but seems rather centered (Fig. 2(c)). The relative percentage of single-phase nanoparticles, grown following the homogeneous decomposition of  $\text{Fe}(\text{CO})_5$ , is approximately 10% and affects the magnetic features of the sample slightly.

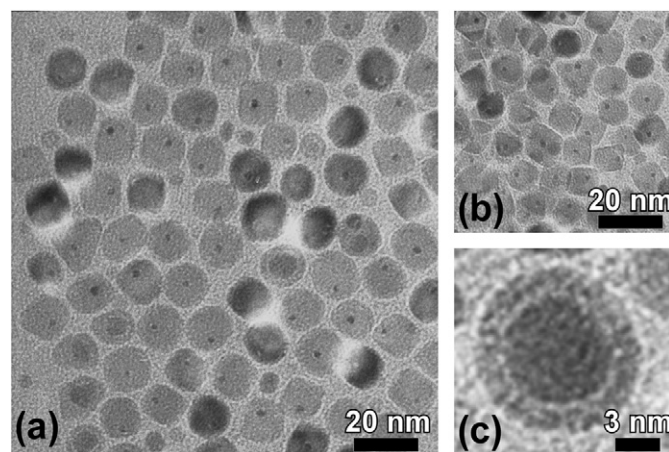


Fig. 2. Low-magnification HRTEM images of heterogeneously nucleated nanoparticles in the final (a) and the intermediate product (b). Overgrown core in an individual nanoparticle (c).

Although the slight increment of the mean diameter in the final product is equal to the doubling of the size in terms of volume, it is far from the expected value according to the quantity of iron precursor added in the second stage. The low yield of the second-stage reaction is explained by the partial consumption of iron precursor in a parallel homogeneous growth of iron oxide nanoparticles. TEM images indicate that such nanoparticles exist even before the second stage and lead to a variation of the size distribution to lower diameters (Fig. 3b).

The undesirable growth of iron nanoparticles by a homogeneous supersaturation route possibly takes place during reflux when both growth and nucleation mechanisms occur. However, in this case, where the aim is the synthesis of relatively large nanoparticles, higher temperatures and certain reflux times are unavoidable, thus the effect is more significant in monodispersity. The presence of such particles indicates that the homogeneous nucleation synthesis under similar conditions would result in smaller nanoparticles because of the low surfactant-to-iron precursor ratio and the higher energy that is required for the initiation of growth. The production of spinel iron oxide nanoparticles larger than 13 nm without Pt seeds requires a surfactant-to-precursor ratio of at least 4:1 in the first stage and similar thermal aging conditions as well as a higher excess of iron precursor than for a heterogeneous procedure in the second stage [17].

Further investigation of single nanoparticles via SAED patterns (Fig. 4) revealed that the shell of large-size nanoparticles as well as the fraction of small nanoparticles consists of very well crystallized iron oxide. Although natural oxidation is difficult to be controlled for the formation of  $\gamma\text{-Fe}_2\text{O}_3$  versus  $\text{Fe}_3\text{O}_4$  there are some indications that the main part is magnetite. The titration analysis of  $\text{Fe}^{2+}$  and  $\text{Fe}^{3+}$  determined the percentage of magnetite as at least 80%. Low maghemite's content is also suggested by the absence of its characteristic (1 1 0) reflection, unlike cases where it is the dominant phase.

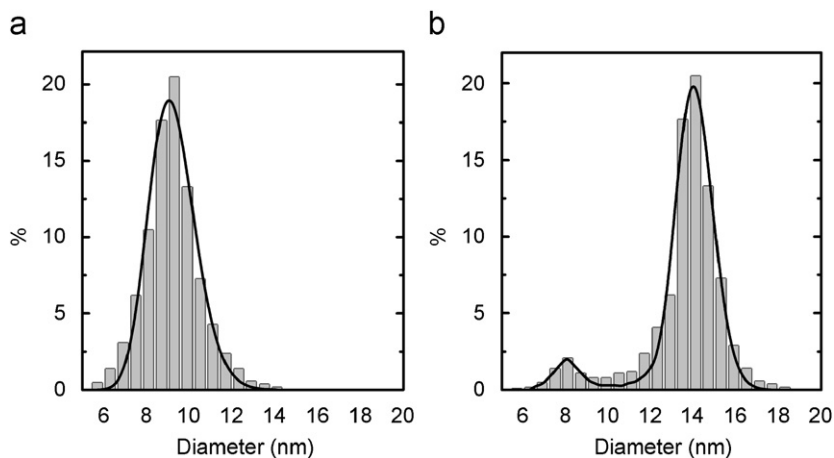


Fig. 3. Size distribution graphs of heterogeneously nucleated nanoparticles after first stage (a) and second stage (b) of growth.

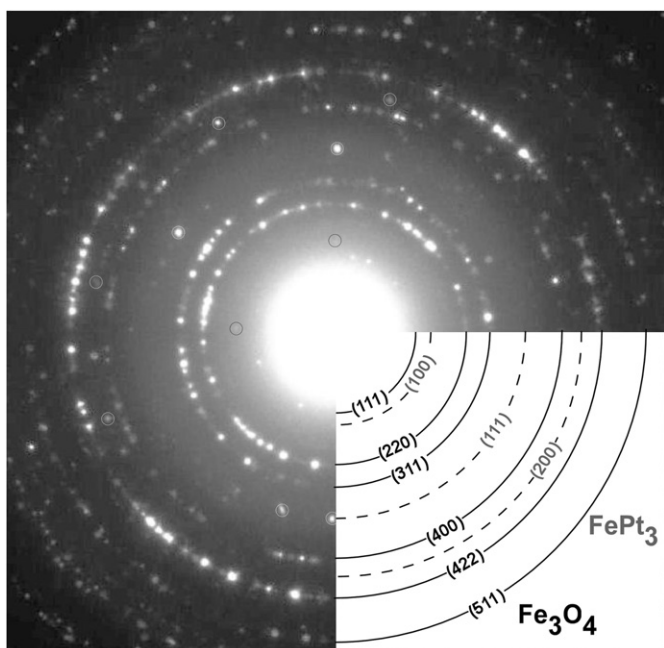


Fig. 4. Electron diffraction pattern of heterogeneously nucleated iron oxide nanoparticles.

We have shown that under similar conditions iron is spontaneously converted to magnetite rather than maghemite [14]. In agreement with this, Sun et al. [18] reported that magnetite is usually the product of iron oxidation when it takes place at room temperature. However, in spite of the experimental indications, we consider these nanoparticles generally as spinel iron oxides. In any case, such a consideration does not affect our discussion.

On the other hand, the core of large nanoparticles does not consist of pure platinum but a platinum-rich Fe–Pt alloy that remains embedded in the center. Platinum (111) and (200) crystal planes appear shifted and coincide with the corresponding values of disordered FePt<sub>3</sub> phase. This fact proves that Pt seeds initially act like catalytic centers for the nucleation of iron but finally they participate in the formation of a magnetic phase that may affect the observed

magnetic properties. The atomic diffusion of iron in platinum core requires thermal energy, which is available at relatively high temperatures. Despite the core being covered by a thick oxide shell, lattice fringes belonging to the FePt<sub>3</sub> structure are visible in some nanoparticles, as the HRTEM image of Fig. 5(a) indicates. The measured *d* spacing of 0.193 nm corresponds to (200) lattice planes of the cubic FePt<sub>3</sub> phase, whereas the (311) planes of Fe<sub>3</sub>O<sub>4</sub> (*d*<sub>311</sub> = 0.253 nm) are mainly observed in the shell or in homogeneously nucleated particles (Fig. 5(b)).

Fig. 6 suggests a possible mechanism of heterogeneous synthesis of large iron oxide nanoparticles. Platinum nuclei are formed at lower temperatures by the reduction of Pt(acac)<sub>2</sub> (Fig. 6(a)). During the first stage of synthesis, amorphous iron coats Pt seeds (Fig. 6(b)) and atomic diffusion of Fe takes place when the temperature reaches the boiling point of dioctyl ether (Fig. 6(c)). After adding an excess of iron precursor and raising the temperature, enlargement of nanoparticles and Fe enrichment of the core continues until the end of the process (Fig. 6(d)). Finally, natural oxidation of iron and crystallization in inverse spinel structure occur immediately after exposure to ambient conditions (Fig. 6(e)). This pathway resembles the formation mechanism of FePt/Fe<sub>3</sub>O<sub>4</sub> core-shell nanoparticles proposed by Chen et al. [19].

### 3.3. FT-IR spectrometry

FT-IR analysis of the powder from the final product provides additional information for iron oxide identification and the organic coating of nanoparticles as well. The wide peak that the sample presents at 590 cm<sup>-1</sup> is similar to the standard spectrum of Fe<sub>3</sub>O<sub>4</sub> (Aldrich, >98%) as the corresponding  $\gamma$ -Fe<sub>2</sub>O<sub>3</sub> (Alfa, 99+%) consists of multiple peaks in the range 580–650 cm<sup>-1</sup> (Fig. 7(b)). The broadening of the peak corresponding to Fe<sub>3</sub>O<sub>4</sub> is attributed to the existence of surfactants and traces of the organic solvent. The Fe–O stretching of magnetite is also evidenced by the pair of lower wavelength bands at 395 and 450 cm<sup>-1</sup>, unlike maghemite, which presents only one [20]. This may

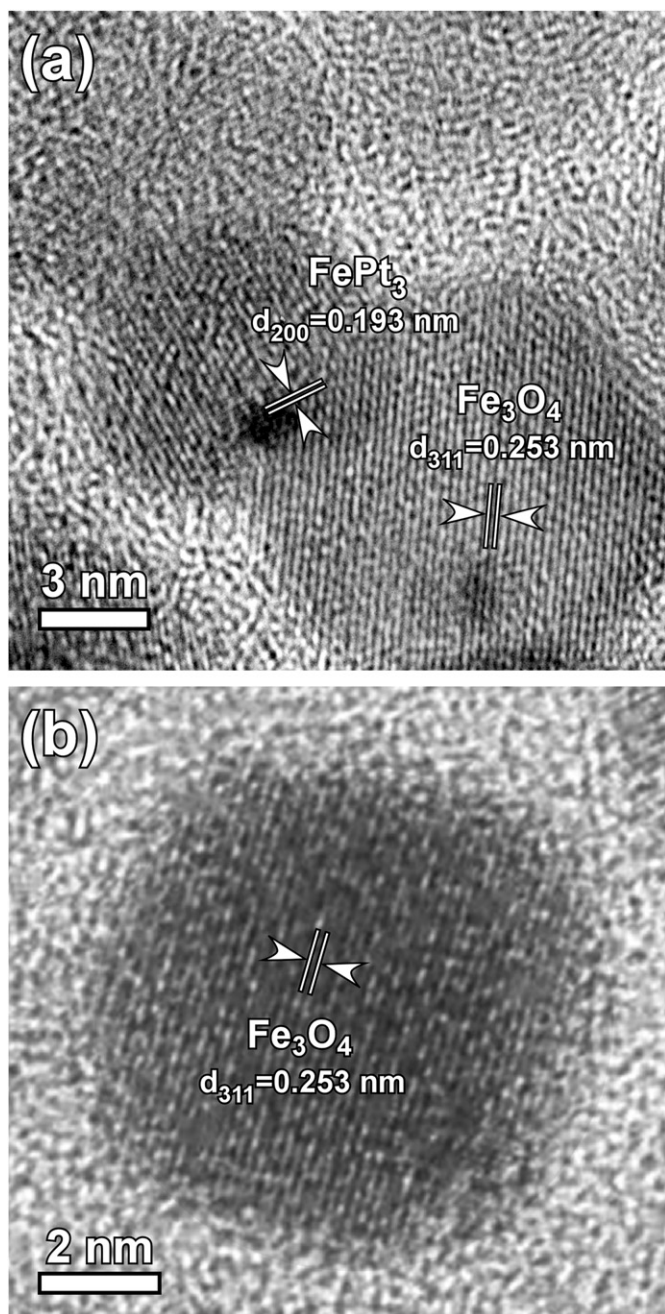


Fig. 5. HRTEM images of heterogeneously (a) and homogeneously (b) nucleated  $\text{Fe}_3\text{O}_4$  nanoparticles.

be due to the fact that magnetite consists of both  $\text{Fe}^{2+}$  and  $\text{Fe}^{3+}$ , whereas maghemite contains only  $\text{Fe}^{3+}$ .

Fig. 7(a) shows the FT-IR spectrum of the synthesized Pt-nucleated  $\text{Fe}_3\text{O}_4$  nanoparticles in the 1000–3500  $\text{cm}^{-1}$  region. For comparison, the spectrum of 13 nm  $\text{Fe}_3\text{O}_4$  nanoparticles, prepared by the homogeneous route, with only oleic acid added, is also given. The strong  $\text{CH}_2$  peaks at 2925 ( $\nu_{\text{as}} \text{C-H}$ ), 2855 ( $\nu_{\text{s}} \text{C-H}$ ) and 1435 ( $\delta_{\text{s}} \text{C-H}$ )  $\text{cm}^{-1}$  as well as the one at 1620  $\text{cm}^{-1}$  ( $\nu \text{C}=\text{C}$ ) are indicative of both molecules of oleic acid and oleylamine [21] that cover the iron oxide nanoparticles. The peak observed at 1705  $\text{cm}^{-1}$  is characteristic of free oleic acid representing the

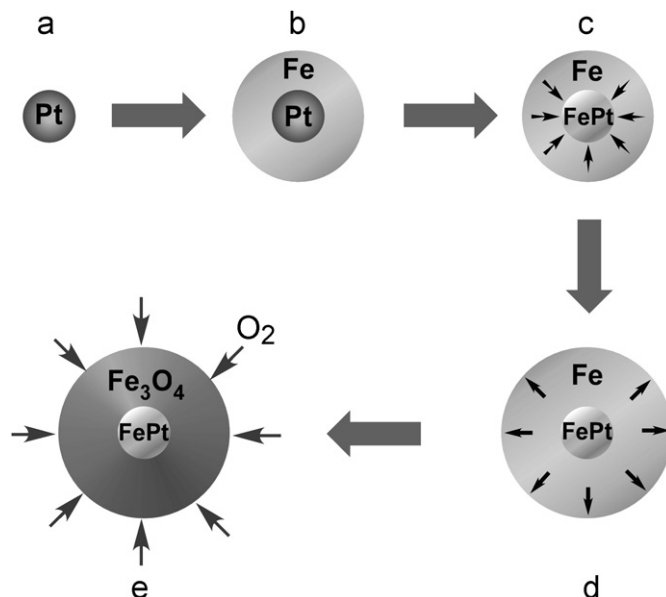


Fig. 6. Schematic demonstration of the heterogeneous synthesis of  $\text{Fe}_3\text{O}_4$  nanoparticles. Formation of Pt seeds (a), nucleation and growth of Fe during first stage (b), diffusion of Fe in the core at high temperatures (c), Fe shell enlargement during second stage (d) and oxidation of Fe shell after exposure to atmosphere (e).

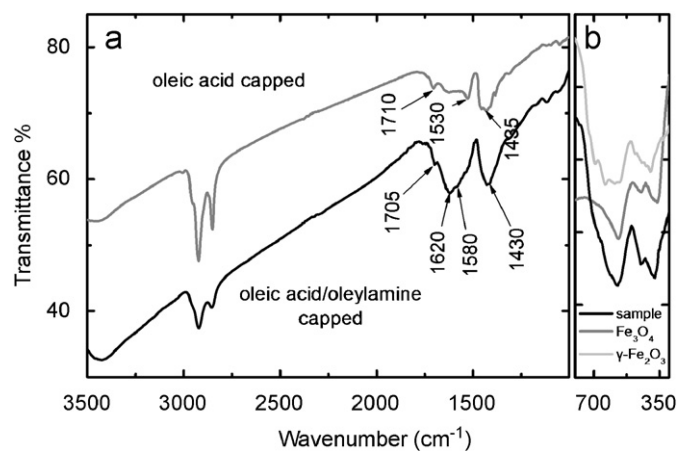


Fig. 7. FT-IR spectra of oleic acid/oleylamine capped heterogeneously nucleated and oleic acid capped homogeneously grown  $\text{Fe}_3\text{O}_4$  nanoparticles (a). Magnified area of the spectrum at low wavenumbers in comparison to magnetite and maghemite (b).

$\text{C}=\text{O}$  asymmetric vibration. It is attributed to the physically adsorbed oleic acid remaining on the nanoparticle surface after washing and redispersion process. The band at 1530  $\text{cm}^{-1}$  appears due to the  $\text{C}-\text{O}$  bond, indicating that oleic acid molecules are covalently bonded to the nanoparticle surface. The presence of oleylamine is evidenced by the peak lying at 1580  $\text{cm}^{-1}$  as a result of intact adsorption of  $\text{NH}_2$  onto the particle [22].

#### 3.4. TGA measurement

Fig. 8 shows the TGA for the nanoparticles obtained after the second stage. The initial loss observed up to

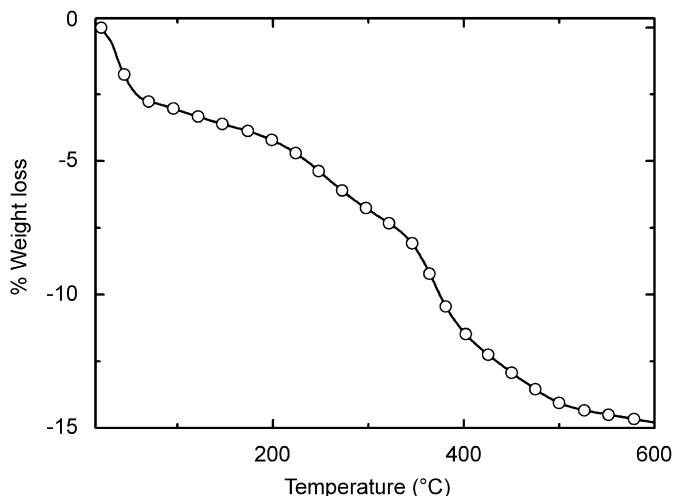


Fig. 8. Temperature dependence of weight loss of heterogeneously nucleated  $\text{Fe}_3\text{O}_4$  nanoparticles.

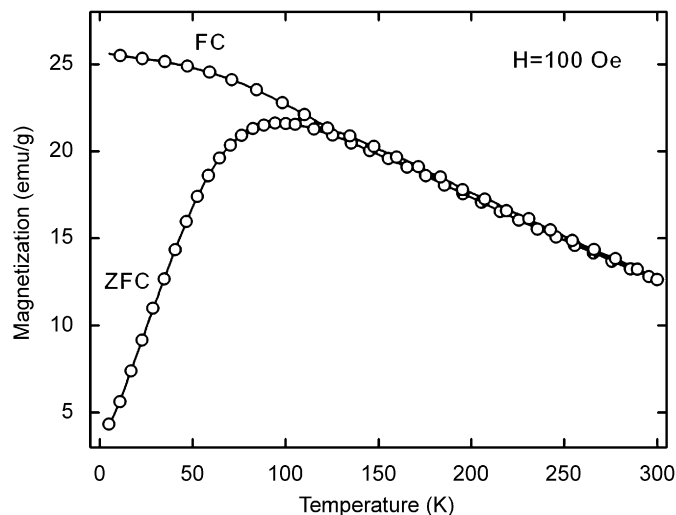


Fig. 9. Zero-field cooling (ZFC) and field-cooling (FC) curves of heterogeneously nucleated  $\text{Fe}_3\text{O}_4$  nanoparticles under 100 Oe.

100 °C corresponds to humidity or to residual solvent molecules adsorbed in the powder. From 150 to 400 °C, decomposition of the capping agents takes place. Weight loss measured 13%, indicating the percentage of organic surfactants in the sample. This is equal to the value for the full coverage of the surface of 14 nm spherical nanoparticles by a monolayer of oleic acid and oleylamine.

Even though complete removal of free oleic acid is expected at 260 °C [23], significant quantities of surfactants remain till 500 °C owing to their strong linkage on the particle surface. The variation in loss rate is due to the difference in the strength of the surfactant-to-metal bond between oleic acid and oleylamine as well as to possible changes in their chain structure introduced at temperatures over 300 °C.

### 3.5. Magnetic characterization

The temperature dependence of the magnetization under ZFC and FC conditions for the second-stage product is shown in Fig. 9 in the range 5–300 K. The behavior of the two curves is typical for superparamagnetic iron oxide nanoparticles in spite of the presence of the Pt-rich core [17]. The initial magnetization in the ZFC branch at low temperatures reaches zero, reflecting the demagnetized state of the nanoparticles due to absence of an external field. Increasing the temperature, in combination with an applied field of 100 Oe, results in a constant increase of total magnetization, as more nanoparticles can overcome their energy barrier and orientate their moments toward the external field. ZFC curve presents a rounded maximum at the temperature  $T_{\text{max}} = 97$  K, after which thermal activation energy is sufficient to induce transition from ferrimagnetism to superparamagnetism. In fact, this broad peak indicates the distribution in blocking temperatures over a wide range of different particle sizes or anisotropies

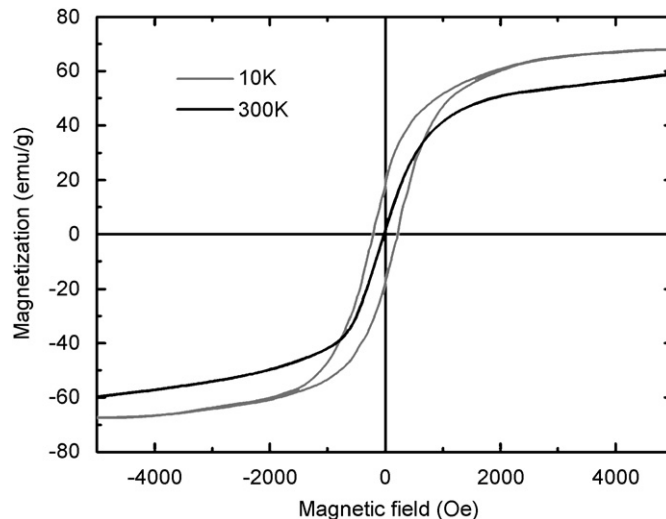


Fig. 10. Hysteresis loops of heterogeneously nucleated  $\text{Fe}_3\text{O}_4$  nanoparticles at 10 and 300 K.

[24]. In addition, the fraction of small homogeneously nucleated nanoparticles and the  $\text{FePt}_3$  core may contribute to the shift of the peak.

For an assembly of nanoparticles with log-normal size distribution, the mean blocking temperature can be found by  $T_b = T_{\text{max}}/c$ , where  $c \approx 1.5$  [25]. Considering that the homogeneously grown particle fraction is small enough and the Pt-rich core represents only 1% in mass of the heterogeneously nucleated particles,  $T_b$  should be close to the calculated value of 65 K. Compared to magnetite nanoparticles of similar size that have been studied, such a low temperature may be attributed to the reduction of particle interactions and surface anisotropy [23]. Surfactant coating prevents any kind of aggregation and nanoparticles can freely align to the external field. The effective anisotropy constant is found by applying the equation

$K_{\text{eff}} = 25k_{\text{B}}T_{\text{b}}/V$  [26], where  $k_{\text{B}}$  is Boltzmann's constant and  $V$  the mean particle volume excluding the Pt-rich core. The  $K_{\text{eff}}$  value ( $1.6 \times 10^5 \text{ erg cm}^{-3}$ ) is slightly higher than the corresponding value of bulk magnetite ( $1.3 \times 10^5 \text{ erg cm}^{-3}$ ), possibly due to shape anisotropy arising from the polygonal shape of nanoparticles.

After reaching the maximum magnetization value, ZFC curve follows a decreasing path till room temperature, indicating a Curie's law behavior [10]. This steady reduction implies physical isolation between the nanoparticles due to the oleic acid coating on their surface and consequently their fine dispersion [27]. In the case of field cooling, the curve gets its maximum value at 5 K and then linearly decreases with rising temperature, coinciding with ZFC curve over 140 K. After this point, all nanoparticles display superparamagnetic relaxation. The divergence of ZFC and FC curves below separation temperature is attributed to the existence of a magnetic anisotropy energy barrier that prevents magnetization reversal [28].

The magnetic hysteresis loops of the same sample were recorded for the temperatures of 10 and 300 K (Fig. 10). In principle, the characteristics of each loop verify the discussion on ZFC–FC measurements. The sample shows its ferrimagnetism at 10 K, which is fairly below the blocking temperature, having a coercivity value of 217 Oe and about 15 emu/g of remanence. On the other hand, nanoparticles are typically superparamagnetic at room temperature, as the zero coercivity and the absence of saturation indicate. The saturation magnetization at 300 K reaches 59 emu/g, which is very close to iron oxide samples of similar size [14], but only 65% of bulk magnetite (90 emu/g). The reason for this declination is the appearance of spin canting effects due to crystal size decreasing and the existence of the surfactant at nanoparticle surface [29]. However, the improved crystallinity of nanoparticles restrains this tendency and maintains saturation magnetization at high values. The value at 10 K is higher (67 emu/g) as the effect of thermal fluctuations is reduced under the superparamagnetic limit.

The magnetic particle diameter  $D_{\text{M}}$  has been obtained by applying Chantrell's equation [30] using the 300 K magnetization curve, assuming zero interaction between nanoparticles and a log-normal size distribution:

$$D_{\text{M}} = \left[ \frac{18 k_{\text{B}} T}{\pi M_{\text{s}}} \sqrt{\frac{\chi_{\text{i}}}{3m_{\text{s}}H_0}} \right]^{1/3}, \quad (1)$$

where  $M_{\text{s}}$  and  $m_{\text{s}}$  are the saturation magnetization of the bulk magnetite and the nanoparticles, respectively,  $\chi_{\text{i}}$  is the initial susceptibility and  $T$  the temperature.  $H_0$  is calculated by extrapolating the linear part of  $M-1/H$  curve to the  $1/H$  axis at  $M=0$ . Taking into account the multi-phase character and the bimodal distribution of the second-stage product, the value of 12.4 nm that is calculated is in good agreement with TEM data, indicating the independent rotation of nanoparticle magnetic moments.

#### 4. Conclusion

The preparation of  $\text{Fe}_3\text{O}_4$  nanoparticles as large as 14 nm, applying a two-stage heterogeneous growth on Pt seeds, was achieved by increasing the duration of heating at high temperatures. The low percentage of Pt in the sample does not affect the macroscopically observed properties, whereas it participates in the growth mechanism. During the first stage Pt seeds operate as nucleation centers for iron growth. The result of diffusion that takes place at the boiling point is the formation of a Pt-rich Fe–Pt alloy core inside each nanoparticle.

Although this process leads to a less monodispersed product, the enlargement of nanoparticles is accompanied by a fine isolation originating from the surfactant monolayer, which completely surrounds each one of them. The good agreement in the calculation of the mean nanoparticle diameter by TEM, XRD and magnetic measurements proves their high crystallinity and the absence of magnetic interactions between them.

#### Acknowledgment

This work was supported by the Greek Secretariat of Research and Technology—Contract no. 03ED667.

#### References

- [1] A.-H. Lu, E.L. Salabas, F. Schuth, *Angew. Chem. Int. Ed.* 46 (2007) 1222.
- [2] Y. Qiang, J. Antony, A. Sharma, J. Nutting, D. Sikes, D. Meyer, *J. Nanopart. Res.* 8 (2006) 489.
- [3] Q.A. Pankhurst, J. Connolly, S.K. Jones, J. Dobson, *J. Phys. D* 36 (2003) R167.
- [4] N.A. Peppas, *Adv. Drug Deliver. Rev.* 56 (2004) 1529.
- [5] A. Ito, M. Shinkai, H. Honda, T. Kobayashi, *J. Biosci. Bioeng.* 100 (2005) 1.
- [6] S. Sun, C.B. Murray, D. Weller, L. Folks, A. Moser, *Science* 287 (2000) 1989.
- [7] D.J. Sellmyer, *Nature* 420 (2002) 374.
- [8] X. Teng, D. Black, N.J. Watkins, Y. Gao, H. Yang, *Nano Lett.* 3 (2003) 261.
- [9] H. Zeng, J. Li, J.P. Liu, Z.L. Wang, S. Sun, *Nature* 420 (2002) 395.
- [10] D.L. Huber, *Small* 1 (2005) 482.
- [11] A.C.S. Samia, J.A. Schlueter, J.S. Jiang, S.D. Bader, C.-J. Qin, X.-M. Lin, *Chem. Mater.* 18 (2006) 5203.
- [12] P. Tartaj, M.P. Morales, S. Veintemillas-Verdaguer, T. Gonzalez-Carreno, C.J. Serna, *J. Phys. D* 36 (2003) R182.
- [13] D. Farrell, S.A. Majetich, J.P. Wilcoxon, *J. Phys. Chem. B* 107 (2003) 11022.
- [14] K. Simeonidis, S. Mourdikoudis, M. Moulla, I. Tsiaoussis, C. Martinez-Boubeta, M. Angelakeris, C. Dendrinos-Samara, O. Kalogirou, *J. Magn. Magn. Mater.* 316 (2007) e1.
- [15] H. Zeng, J. Li, Z.L. Wang, J.P. Liu, S. Sun, *Nano Lett.* 4 (2004) 187.
- [16] H. Yu, M. Chen, P.M. Rice, S.X. Wang, R.L. White, S. Sun, *Nano Lett.* 5 (2005) 379.
- [17] C. Martinez-Boubeta, K. Simeonidis, M. Angelakeris, N. Pazos-Perez, M. Giersig, A. Delimitis, L. Nalbandian, V. Alexandrakis, D. Niarchos, *Phys. Rev. B* 74 (2006) 054430.
- [18] S. Sun, H. Zeng, D.B. Robinson, S. Raoux, P.M. Rice, S.X. Wang, G. Li, *J. Am. Chem. Soc.* 126 (2004) 273.

- [19] M. Chen, J.P. Liu, S. Sun, *J. Am. Chem. Soc.* 126 (2004) 8394.
- [20] K. Simeonidis, S. Mourdikoudis, I. Tsiaoussis, N. Frangis, M. Angelakeris, O. Kalogirou, A. Delimitis, C. Dendrinou-Samara, *Mod. Phys. Lett. B* 21 (2007) 1143.
- [21] S.Y. Lee, M.T. Harris, *J. Colloid Interface Sci.* 293 (2006) 401.
- [22] N. Shukla, C. Liu, P.M. Jones, D. Weller, *J. Magn. Magn. Mater.* 266 (2003) 178.
- [23] A.G. Roca, M.P. Morales, K. O'Grady, C.J. Serna, *Nanotechnology* 17 (2006) 2783.
- [24] L. Zhang, G.C. Papaefthymiou, J.Y. Ying, *J. Phys. Chem. B* 105 (2001) 7414.
- [25] F. Cattaruzza, D. Fiorani, A. Flamini, P. Imperatori, G. Scavia, L. Suber, A.M. Testa, A. Mezzi, G. Ausanio, W.R. Plunkett, *Chem. Mater.* 17 (2005) 3311.
- [26] W.F. Brown, *Phys. Rev.* 130 (1963) 1677.
- [27] S.H. Im, T. Herricks, Y.T. Lee, Y. Xia, *Chem. Phys. Lett.* 401 (2005) 19.
- [28] A.J. Rondinone, A.C.S. Samia, A.J. Zhang, *J. Phys. Chem. B* 103 (1999) 6876.
- [29] R.H. Kodama, A.E. Berkowitz, E.J. McNiff, S. Foner, *Phys. Rev. Lett.* 77 (1996) 394.
- [30] R.W. Chantrell, J. Popplewell, S.W. Charles, *IEEE Trans. Magn.* 14 (1978) 975.